A three-dimensional vector radiative transfer (3D-VRT) equation for inhomogeneous scatter media*

JIN Yaqiu** and LIANG Zichang

(Center for Wave Scattering and Remote Sensing and School of Information Science and Engineering, Fudan University, Shanghai 200433, China)

Received March 25, 2003; revised May 20, 2003

Abstract To solve 3D-VRT equation for the model of spatially inhomogeneous scatter media, the finite enclosure of the scatter media is geometrically divided, in both the vertical z and horizontal (x, y) directions, to form very thin multi-boxes. The zero-th order emission, first-order Mueller matrix of each thin box and an iterative approach of high-order radiative transfer are applied to deriving high-order scattering and emission of whole inhomogeneous scatter media. Numerical results of polarized brightness temperature at microwave frequency from inhomogeneous scatter model such as vegetation canopy are calculated and discussed.

Keywords: inhomogeneous media, 3D-VRT, high-order scattering and emission.

To describe multiple scattering, absorption and emission of radiance intensity, the vector radiative transfer (VRT) equation of the Stokes vector $\boldsymbol{I}$ has been studied and applied in broad areas. Conventional VRT is usually for the models of parallel-layered media, i. e. one-dimensional (1D) VRT equation $(\mathrm{d}\boldsymbol{I}/\mathrm{d}z)$[1, 2]. There have been some studies of 2D or 3D scalar RT equations, such as the Monte Carlo method and multi-modes approach for radiance of atmospheric discrete clouds[3~6], the discrete-ordinate and finite difference method for the problems of heat transfer[7, 8] and neutron transport etc. However, in all of these approaches it has been necessary to assume that the host medium itself is homogeneous, i.e. extinction, scattering and phase functions are considered to be independent of location within the medium. This fact simplifies the problem somewhat as the inhomogeneity in RT and then requires only a suitable treatment of the lateral sides of the medium and their associated boundary conditions. In advances of polarimetric and radiometric observation in remote sensing and the imaginary technology with an improved high resolution, development of 3D-VRT ($\mathrm{d}\boldsymbol{I}/\mathrm{d}x$, $\mathrm{d}\boldsymbol{I}/\mathrm{d}y$, $\mathrm{d}\boldsymbol{I}/\mathrm{d}z$) model for spatially inhomogeneous scatter media such as vegetation canopy becomes of great interest[9~11]. However, modeling and numerical solution of 3D-VRT for inhomogeneous scatter media remains to be studied.

To solve 3D-VRT equation for spatially inhomogeneous scatter media and obtain high-order scattering and emission, the finite enclosure of the scatter media is first geometrically divided into many thin boxes, slicing the media in both the vertical z and horizontal (x, y) directions. The zero-th order emission of each thin box and an iterative approach of high-order radiative transfer via the Mueller matrix solution of VRT in all media boxes are applied to deriving high-order scattering and emission of whole inhomogeneous scatter media. High order scattering and brightness temperature of the inhomogeneous scatter media in 3D geometry can be numerically calculated. According to the spatial resolution of the observation to divide the finite enclosure of scatter media, this approach presents numerical method to obtain high-order scattering and emission of the 3-D models for inhomogeneous scatter media such as vegetation canopy, finite cloud fields etc.

1 The 3D-VRT equation

A geometric model is shown in Fig. 1, where non-spherical particles are randomly and non-uniformly distributed within random limited space, e.g. such as random cones (it might be as a model for random tree canopy or others). Suppose that the finite enclosure of the media has the length and width as W_1 and W_2, in the x and y directions respectively, and the

* Supported by the Major State Basic Research Development Program of China (2001CB309401) and the National Natural Science Foundation of China (Grant No. 60171009)

** To whom correspondence should be addressed. E-mail: yqjin@fudan.ac.cn

height d in the z direction. Note that in this model the top and lateral boundaries of the enclosure are not solid, and the underneath of the bottom surface is a homogeneous half-space (land-) medium. The 3D-VRT[8, 10, 12] of the random scatter media is written as

$$\left(\cos\theta\frac{\partial}{\partial z}+\sin\theta\cos\varphi\frac{\partial}{\partial x}+\sin\theta\sin\varphi\frac{\partial}{\partial y}\right)\cdot\boldsymbol{I}(\theta,\varphi,x,y,z)$$
$$=-\bar{\bar{\kappa}}_e(\theta,\varphi,x,y,z)\cdot\boldsymbol{I}(\theta,\varphi,x,y,z)+\bar{\bar{\kappa}}_a(\theta,\varphi,x,y,z)\cdot C\boldsymbol{T}_1(x,y,z)+\int_0^{2\pi}\mathrm{d}\varphi'\int_0^{\pi}\bar{\boldsymbol{P}}(\theta,\varphi,\theta',\varphi',x,y,z)\cdot\boldsymbol{I}(\theta',\varphi',x,y,z)\sin\theta'\mathrm{d}\theta', \quad (1)$$

where $\bar{\bar{\kappa}}_e$, $\bar{\bar{\kappa}}_a$ are, respectively, the extinction and absorption matrices, $\bar{\boldsymbol{P}}$ is the phase matrix, and $\boldsymbol{T}_1$ is the physical temperature of the scatter media.

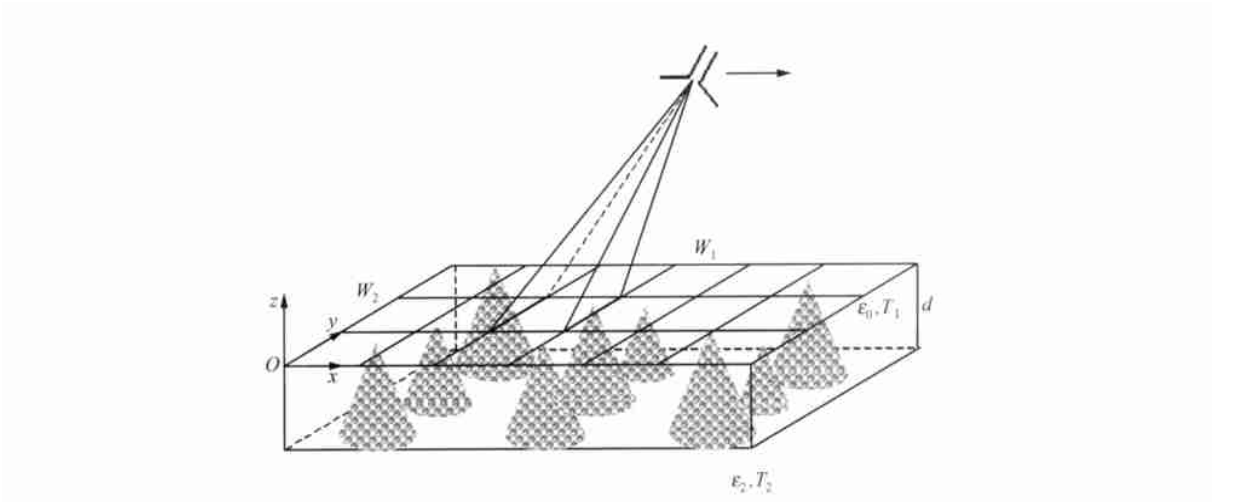

Fig. 1. A geometric model for inhomogeneous scatter media.

The boundary conditions at the top ($z=0$) and bottom ($z=-d$) surfaces are written as

$$\boldsymbol{I}(\pi-\theta,\varphi,x,y,z=0)=0, \quad (2a)$$

$$\boldsymbol{I}(\theta,\varphi,x,y,z=-d)=\bar{\boldsymbol{R}}_{12}(\theta)\cdot\boldsymbol{I}(\pi-\theta,\varphi,x,y,z=-d)+\bar{\boldsymbol{T}}_{12}(\theta)\cdot C\boldsymbol{T}_2, \quad (2b)$$

where $\bar{\boldsymbol{R}}_{12}(\theta)$, $\bar{\boldsymbol{T}}_{12}(\theta)$ are the reflectivity and transmittivity matrices of the bottom surface, respectively. Here, the subscript 12 denotes "between" the random media (1) and underlying medium (2). T_2 is the physical temperature of the bottom medium. Eq. (2a) means that there is no downwards emission incidence at $(\pi-\theta,\varphi)$ from up-space ($z>0$) to the top surface ($z=0$). Eq. (2b) indicates that the upwards radiance at the bottom ($z=-d$) is contributed by reflection of downwards radiance of the random media and transmitted emission from the underlying medium.

The boundary conditions at the lateral surfaces at $x=0$, $x=W_1$, $y=0$ and $y=W_2$ are respectively written as

$$\begin{cases}\boldsymbol{I}(\pi-\theta,\varphi,x=0,y,z)=0,\\ \boldsymbol{I}(\theta,\varphi,x=0,y,z)=\bar{\boldsymbol{T}}_{12}(\theta)\cdot C\boldsymbol{T}_2,\end{cases} \quad 0^\circ<\varphi<90^\circ,\ 270^\circ<\varphi<360^\circ, \quad (2c)$$

$$\begin{cases}\boldsymbol{I}(\pi-\theta,\varphi,x=W_1,y,z)=0,\\ \boldsymbol{I}(\theta,\varphi,x=W_1,y,z)=\bar{\boldsymbol{T}}_{12}(\theta)\cdot C\boldsymbol{T}_2,\end{cases} \quad 90^\circ<\varphi<270^\circ, \quad (2d)$$

$$\begin{cases}\boldsymbol{I}(\pi-\theta,\varphi,x,y=0,z)=0,\\ \boldsymbol{I}(\theta,\varphi,x,y=0,z)=\bar{\boldsymbol{T}}_{12}(\theta)\cdot C\boldsymbol{T}_2,\end{cases} \quad 0^\circ<\varphi<180^\circ, \quad (2e)$$

$$\begin{cases}\boldsymbol{I}(\pi-\theta,\varphi,x,y=W_2,z)=0,\\ \boldsymbol{I}(\theta,\varphi,x,y=W_2,z)=\bar{\boldsymbol{T}}_{12}(\theta)\cdot C\boldsymbol{T}_2,\end{cases} \quad 180^\circ<\varphi<360^\circ. \quad (2f)$$

Eq. (2c) indicates that there is no downwards incidence from outside to enter the lateral side ($x=0$ and defined by φ region) of the random media, and the upwards radiance from outside comes from the transmitting emission from the underlying half-space medium. The same physical meanings are described by Eqs. (2d, e, f) for other lateral sides.

Generally, $\bar{\bar{\kappa}}_e$ is non-diagonal for non-uniformly (the Euler angles β, γ)[11] oriented scatterers. To find the matrix $\bar{\boldsymbol{E}}$ and its inverse $\bar{\boldsymbol{E}}^{-1}$, $\bar{\bar{\kappa}}_e$ can be diagnosed for uniformly γ-oriented ($\gamma\in(0^\circ,360^\circ)$) scatterers as[1, 2, 13]:

$$\bar{\bar{\beta}}(\theta,\varphi,x,y,z)=\bar{\boldsymbol{E}}^{-1}(\theta,\varphi,x,y,z)\cdot\bar{\bar{\kappa}}_e(\theta,\varphi,x,y,z)\cdot\bar{\boldsymbol{E}}(\theta,\varphi,x,y,z), \quad (3)$$

where the ii-th elements of the diagonal $\bar{\bar{\beta}}$ is denoted as β_i, $i=1,2,3,4$. It can be known that β_i is the

eigen-values of $\bar{\bar{\kappa}}_e$, and $\boldsymbol{E}$ is composed by the eigen-vectors of $\bar{\bar{\kappa}}_e$. All formulations of $\bar{\bar{\kappa}}_e$, $\bar{\bar{\beta}}$ and $\boldsymbol{E}$ can be found in Refs. [1, 2].

Left-multiplying $\boldsymbol{E}^{-1}$ on both sides of Eq. (1) yields

$$\left(\cos\theta\frac{\partial}{\partial z}+\sin\theta\cos\varphi\frac{\partial}{\partial x}+\sin\theta\sin\varphi\frac{\partial}{\partial y}\right)\circ\boldsymbol{I}^E(\theta,\varphi,x,y,z)=-\bar{\bar{\beta}}(\theta,\varphi,x,y,z)\circ\boldsymbol{I}^E(\theta,\varphi,x,y,z)+\bar{\bar{\kappa}}_a^E(\theta,\varphi,x,y,z)\circ\boldsymbol{C}\boldsymbol{T}_0^E(x,y,z)+\int_0^{2\pi}\mathrm{d}\varphi'\int_0^{\pi}\boldsymbol{P}^E(\theta,\varphi,\theta',\varphi',x,y,z)\circ\boldsymbol{I}^E(\theta',\varphi',x,y,z)\sin\theta'\mathrm{d}\theta', \quad (4)$$

where

$$\boldsymbol{I}^E(\theta,\varphi,x,y,z)=\boldsymbol{E}^{-1}(\theta,\varphi,x,y,z)\circ\boldsymbol{I}(\theta,\varphi,x,y,z), \quad (5a)$$

$$\boldsymbol{T}_0^E(x,y,z)=\boldsymbol{E}^{-1}(\theta,\varphi,x,y,z)\circ\boldsymbol{T}_0(x_1,y_1,z), \quad (5b)$$

$$\boldsymbol{P}^E(\theta,\varphi;\theta',\varphi',x,y,z)=\boldsymbol{E}^{-1}(\theta,\varphi,x,y,z)\circ\boldsymbol{P}(\theta,\varphi;\theta',\varphi',x,y,z)\circ\boldsymbol{E}(\theta,\varphi,x,y,z), \quad (5c)$$

$$\bar{\bar{\kappa}}_a^E(\theta,\varphi,x,y,z)=\boldsymbol{E}^{-1}(\theta,\varphi,x,y,z)\circ\bar{\bar{\kappa}}_a(\theta,\varphi,x,y,z)\circ\boldsymbol{E}(\theta,\varphi,x,y,z). \quad (5d)$$

For convenience, notations of E would not be especially indicated in next derivations.

Let us slice the media enclosure into many thin-slabs with the thickness Δd along the z direction, and denote the slabs by the subscripts $l=1, 2, \cdots, L$ from the top to the bottom. According to the spatial resolution Δh, dividing the (x, y) plane of the media enclosure to form many thin rectangular boxes with the length-width Δh and thickness Δd as illustrated in Fig. 2. Because all boxes are very thin, we can assume that the medium within each box is homogeneous. But different boxes can be different, e.g. with different particles, different particle's fractional volumes, or different physical temperatures, etc. It is noted that as the $\bar{\bar{\kappa}}_e$ and $\boldsymbol{P}$ of random particles have been calculated, the approach of VRT of random discrete particles is the same as the one of continuous random media no matter what size the particles are comparing with Δd.

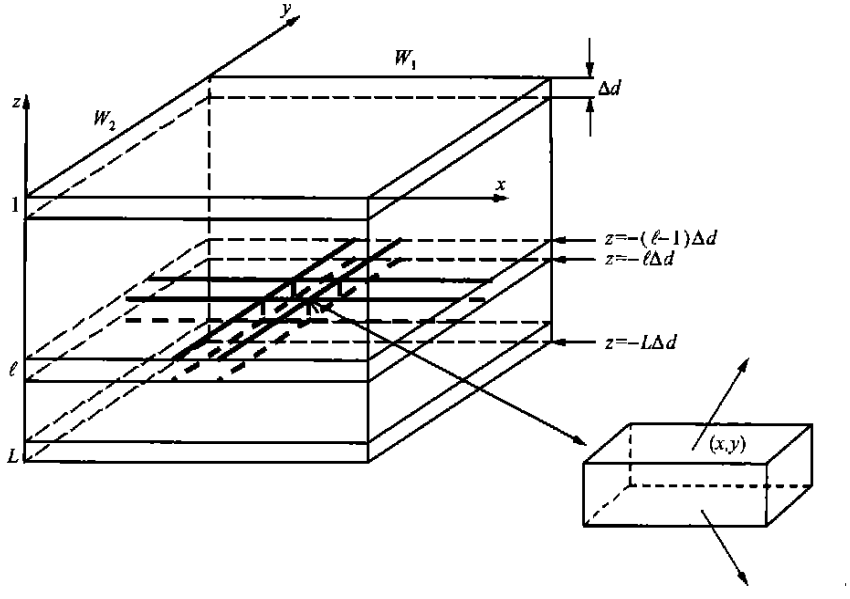

Fig. 2. Dividing the scatter media into multi-boxes.

As illustrated in Fig. 2, the radiance intensity of the l-th slab is defined as

$$\boldsymbol{I}_l(\theta,\varphi,x,y)=\begin{cases}\boldsymbol{I}(\theta,\varphi,x,y,z=-(l-1)\Delta d),\\ \quad 0^\circ<\theta<90^\circ,\\ \boldsymbol{I}(\theta,\varphi,x,y,z=-l\Delta d),\\ \quad 90^\circ<\theta<180^\circ,\end{cases} \quad (6)$$

where $\boldsymbol{I}_l(\theta, \varphi, x, y)$ is the radiance intensity in the direction (θ, φ) from the box of the l-th slab whose center is defined at (x, y).

2 Scattering and radiative transfer of 3D-thin boxes

Because Δd is very small ($\Delta d \ll \Delta h$), change of

the radiance intensity through the lateral sides is always much smaller than the one through the top and bottom surfaces. Thus, based on VRT Eq. (1), the changes of up-going ($0^\circ < \theta < 90^\circ$) and down-going ($90^\circ < \theta < 180^\circ$) radiance intensities through the box of the l-th slab whose center is defined at (x, y) are derived as follows

$$\boldsymbol{I}_l^{(n)}(\theta, \varphi, x+\Delta x, y+\Delta y) = \boldsymbol{I}_{l+1}^{(n)}(\theta, \varphi, x, y)\exp[-\vec{\beta}_l(\theta, \varphi, x, y)\Delta d\sec\theta] + \boldsymbol{I}_{ls}^{(n)}(\theta, \varphi, x+\Delta x, y+\Delta y), \quad (7a)$$

$$\boldsymbol{I}_l^{(n)}(\theta, \varphi, x+\Delta x, y+\Delta y) = \boldsymbol{I}_{l-1}^{(n)}(\theta, \varphi, x, y)\exp[\vec{\beta}_l(\theta, \varphi, x, y)\Delta d\sec\theta] + \boldsymbol{I}_{ls}^{(n)}(\theta, \varphi, x+\Delta x, y+\Delta y), \quad (7b)$$

where $\boldsymbol{I}_{ls}^{(n)}$ is the radiance intensity happening in the box self, where the superscript n indicates the iteration number. $\vec{\beta}_l = [\beta_{1l}, \beta_{2l}, \beta_{3l}, \beta_{4l}]$ is the vector of diagonal $\vec{\beta}$ of the l-th slab.

Radiance transfering from the $(l-1)$-th and $(l+1)$-th slabs can present the following relations:

$$\Delta x = \tan\theta\cos\varphi \cdot \Delta d, \quad \Delta y = \tan\theta\sin\varphi \cdot \Delta d. \quad (8)$$

The zero-th order emission of the box self is

$$\boldsymbol{I}_{ls}^{(n=0)}(\theta, \varphi, x, y) = \frac{1-\exp(-\vec{\beta}_l\Delta d\ |\sec\theta\ |)}{\vec{\beta}_l} \cdot \bar{\bar{\kappa}}_{al}(\theta, \varphi, x, y)\boldsymbol{CT}_{0l}(x, y). \quad (9a)$$

Multiple scattering from all directions under up-going and down-going incidences upon the box is

$$\boldsymbol{I}_{ls}^{(n>0)}(\theta, \varphi, x, y) = \int_0^{2\pi} d\varphi' \int_{\pi/2}^{\pi} \bar{\bar{\boldsymbol{M}}}_l(\theta, \varphi, \theta', \varphi', x', y') \cdot \boldsymbol{I}_{l-1}^{(n-1)}(\theta', \varphi', x', y')\sin\theta' d\theta' + \int_0^{2\pi} d\varphi'' \int_0^{\pi/2} \bar{\bar{\boldsymbol{M}}}_l(\theta, \varphi, \theta'', \varphi'', x'', y'') \cdot \boldsymbol{I}_{l+1}^{(n-1)}(\theta'', \varphi'', x'', y'')\sin\theta'' d\theta'' \quad (9b)$$

and the relations are also given as

$$x' = x + \frac{\Delta x}{2} + \frac{\Delta d\tan\theta'\cos\varphi'}{2}, \quad y' = y + \frac{\Delta y}{2} + \frac{\Delta d\tan\theta'\sin\varphi'}{2}, \quad (10a)$$

$$x'' = x + \frac{\Delta x}{2} - \frac{\Delta d\tan\theta''\cos\varphi''}{2}, \quad y'' = y + \frac{\Delta y}{2} - \frac{\Delta d\tan\theta''\sin\varphi''}{2}. \quad (10b)$$

The Mueller matrix of the l-th slab, $\bar{\bar{\boldsymbol{M}}}_l$, is approximated by the first order Mueller matrix as:

$$M_{ijl}(\theta, \varphi, \theta', \varphi', x, y) \approx M_{ijl}^{(1)}(\theta, \varphi, \theta', \varphi', x, y) = \frac{P_{ijl}(\theta, \varphi, \pi-\theta', \varphi' x, y)\sec\theta}{\beta_{jl}\sec\theta' + \beta_{il}\sec\theta} \cdot \begin{cases} 1-\exp[-\Delta d(\beta_{jl}\sec\theta' + \beta_{il}\sec\theta)] \\ \quad 0^\circ < \theta < 90^\circ, 0^\circ < \theta' < 90^\circ, \\ \exp(-\beta_{jl}\Delta d\sec\theta') - \exp(\beta_{il}\Delta d\sec\theta) \\ \quad 90^\circ < \theta < 180^\circ, 0^\circ < \theta' < 90^\circ, \\ \exp(\beta_{jl}\Delta d\sec\theta') - \exp(-\beta_{il}\Delta d\sec\theta) \\ \quad 0^\circ < \theta < 90^\circ, 90^\circ < \theta' < 180^\circ, \\ 1-\exp[\Delta d(\beta_{jl}\sec\theta' + \beta_{il}\sec\theta)] \\ \quad 90^\circ < \theta < 180^\circ, 90^\circ < \theta' < 180^\circ, \end{cases} \quad (11)$$

where the subscripts $i, j = 1, 2, 3, 4$.

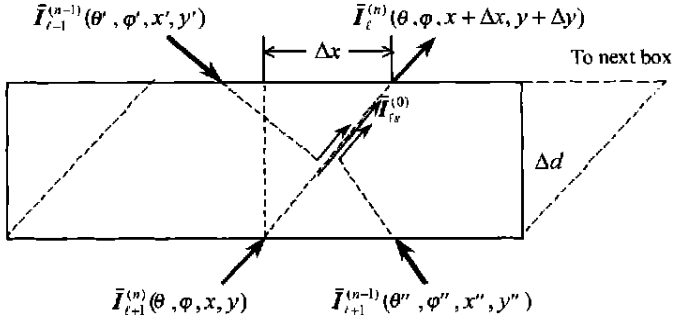

Fig. 3. Illustration of radiative transfer through a box in the *zox* section.

From Fig. 3 and Eq. (7a), it can be seen that the radiance $\boldsymbol{I}_{l+1}^{(n)}(\theta, \varphi, x, y)$ of the box at the center (x, y) becomes $\boldsymbol{I}_l^{(n)}(\theta, \varphi, x+\Delta x, y+\Delta y)$ after propagating and attenuating through this box medium. $\boldsymbol{I}_l^{(n)}(\theta, \varphi, x+\Delta x, y+\Delta y)$ will be distributed and enter into the boxes centers of the $(l-1)$-th slab based on the ray-projected areas.

The thin-lines with arrow in Fig. 3 indicate the zero-th order emission $\boldsymbol{I}_{ls}^{(0)}$ and multiple scattering from the up and bottom interfaces of the box.

Suppose $\Delta h = 100$ cm, $\Delta d = 1$ cm, the calcula-

tion of Eq. (8) yields $\Delta x = 16.5$ cm and $\Delta y = 9.5$ cm for the direction $\theta = 87^\circ$ and $\varphi = 30^\circ$ (noting that the maximum $\theta_M = \cot^{-1}(2\Delta d/\Delta h) \approx 89^\circ$). The result shows that 0.756 of $\boldsymbol{I}_l^{(n)}(\theta, \varphi, x+\Delta x, y+\Delta y)$ remained within the box of the center (x, y), and only 0.079, 0.016, 0.149 of it enter into the neighbor boxes of the centers at $(x, y+\Delta h)$, $(x+\Delta h, y+\Delta h)$, $(x+\Delta h, y)$, respectively. Thus, the radiance intensity through the lateral sides of each box is much smaller than the one through the top and bottom interfaces due to very small Δd, and $\boldsymbol{I}_{ls}^{(n)}$ of Eq. (7) can be calculated by Eqs. (9a, b).

Now the steps to calculate brightness temperature emitted from the top interface $\boldsymbol{T}_B(\theta, \varphi, x, y, z=0)$ is summarized as follows:

(i) By using Eqs. (9a, 11), the zero-th order emission $\boldsymbol{I}_{ls}^{(n=0)}(\theta, \varphi, x, y)$ and the Mueller matrix $\overline{\boldsymbol{M}}_l(\theta, \varphi, \theta', \varphi', x, y)$ of each box are calculated.

(ii) By using the boundary condition (2), calculate the radiative transfer Eq. (7) from the top surface, the slabs $l = 1, 2, \cdots, L$ sequentially, and finally to the bottom surface. Adding the emission and reflection of the bottom surface, calculate the radiative transfer Eq. (7) from the bottom surface, the slabs $l = L, L-1, \cdots, 1$ sequentially, and finally to the top surface. Thus, $\boldsymbol{I}_{l=1}^{(n=0)}(\theta, \varphi, x, y)$ is obtained.

(iii) By using Eq. (9b), calculate the $(n+1)$-th $(n = 0, \cdots)$ order iteration to obtain $\boldsymbol{I}_{ls}^{(n+1)}(\theta, \varphi, x, y)$ of each box.

(iv) Repeating the steps of (ii) and (iii) to the N-th iteration, the calculation is finished when $\boldsymbol{I}_{l=1}^{(N)}(\theta, \varphi, x, y)$ is small enough.

Let $\boldsymbol{I}_{l=1}(\theta, \varphi, x, y)$ be the sum of all iterations $\boldsymbol{I}_{l=1}^{(n)}(\theta, \varphi, x, y)$ $(n = 0, 1, \cdots, N)$. The brightness temperature observed in the up-space is

$$\boldsymbol{T}_B(\theta, \varphi, x, y, z=0) = \frac{1}{C}\boldsymbol{I}_{l=1}(\theta, \varphi, x, y), \quad 0^\circ < \theta < 90^\circ. \tag{12}$$

3 Numerical results

Suppose that the radiometer's frequency is 3GHz, the scatter particles are prolate spheroids with the semi-radii $a = b = 0.1$ cm and $c = 2.5$ cm, the dielectric constant of the particle is $\varepsilon_s = 22 + 5i$, the fractional volume is 0.0003, and spatial orientation distribution of random particles is uniformly over $\beta \in (30^\circ, 60^\circ)$ and $\gamma \in (0^\circ, 360^\circ)$. The dielectric constant of the bottom medium is $\varepsilon_2 = 8 + 1i$. Vertically and horizontally polarized brightness temperatures T_{Bv} and T_{Bh} are calculated.

3.1 Homogeneous media

First, compare the results of 3D-VRT with conventional 1D-VRT for a homogeneous scatter medium. Suppose that random prolate spheroids are uniformly distributed within a rectangular enclosure whose length and width are 15 m, and depth $d = 1$ m. Divide the rectangular enclosure to form thin multi boxes with $\Delta h = 1$ m, $\Delta d = 0.01$ m (i.e. 100 thin slabs), and take calculations at discrete angles $\Delta\theta = 9^\circ$, $\Delta\varphi = 18^\circ$.

From Eqs. (7, 9), it can be seen that rigorous calculation requires the storage of all radiance at different angles (θ, φ) and different centers (x, y) of the boxes. It needs the storage memory of about 144 M. When the media enclosure becomes large, the storage memory would be tremendously increased. To reduce such requirement, we propose to use a parabola line to approximately match the radiance of each slab along all direction (θ, φ), and only store some coefficients of the matching line.

As shown in Figs. 4 (a, b), three matching points of the parabola line are chosen at $z = 0, -d/2, -d$. It only needs to store 3 coefficients from 100 data, and significantly reduces the storage memory to 4M. For example, Figs. 4 (a, b) show the data of 3D-VRT from the slabs, respectively, along the line $(\theta = 58^\circ, \varphi = 9^\circ)$ and $(\pi - \theta = 58^\circ, \varphi = 9^\circ)$, and good matching by a parabola line.

Fig. 5 presents the zero-th order (small black points) and $N = 2$ (big black points) iterative brightness temperatures observed towards the center $(x = 7.5\,\text{m}, y = 7.5\,\text{m}, z = 0)$. Calculation shows that $N = 2$ iteration is good enough in this case. Difference of the radiance of the zero-th order and $N = 2$ results is significant as about 10 K. Because the brightness temperature observed at this center will not be significantly affected by the radiance afar from the lateral sides, as we believed, the result of 3D-VRT is well matched to the result of conventional 1D-VRT[13] (1D means that the enclosure becomes infinite). It numerically validates our 3D-VRT approach.

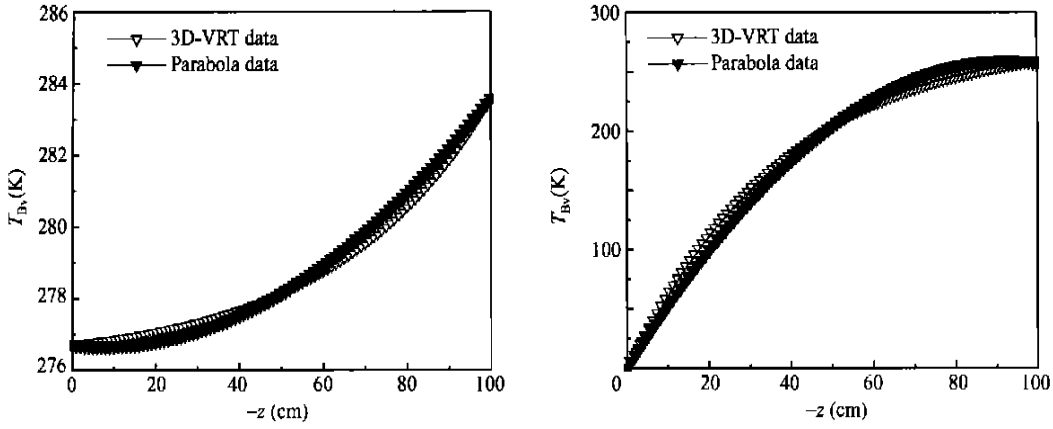

Fig. 4. Parabola data to match the calculation of 3D-VRT.

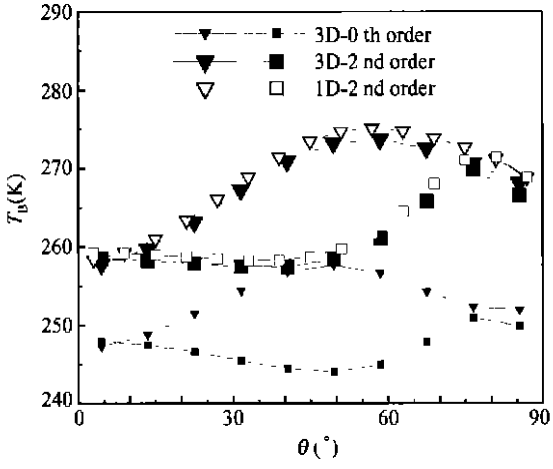

Fig. 5. Brightness temperature from a homogeneous scatter medium.

3.2 Inhomogeneous scatter media

Suppose there is a rectangular enclosure of Fig. 1, whose length and width are 55 m, and the depth $d=4$ m. Spheroid particles are randomly distributed within geometrical cones. The radius and height of the cones randomly take the values of 3~4 m from Monte Carlo realization, and the cone radius is equal to height only for simplicity. Distance between the cones is assumed to be 10 m.

By using the parabola line to reduce the storage (about 58 M), the matching points should be chosen at those locations where there are scatter particles.

Suppose that the radiometer with the spatial resolution Δh at the angle $\theta=58^\circ$, $\varphi=315^\circ$ observes each box one by one. Figs. 6(a, b) show the zero-th order and $N=2$ iterative brightness temperatures. It can be seen that $N=2$ iterative brightness temperature from those locations of random scatter particles significantly enhances the zero-th order emission. Brightness temperature from some parts within the cone locations are higher than the radiance from bottom surface medium because the emission is contributed by random particles, scattering reflected from the bottom surface and the emission from the bottom medium. However, there are also some parts within the cone locations where brightness temperatures become lower because stronger back-scattering of random particles darkens the emission from the bottom medium. On the other hand, because the horizontally polarized brightness temperature from flat bottom surface is low, random particles always enhance brightness temperature within those cone locations.

Fig. 7 shows $N=1$ brightness temperature at a lower frequency 2 GHz, when higher order iteration for weak scattering becomes not necessary. It can be seen that both vertically and horizontally polarized brightness temperatures of random particles of the canopy are higher than the one from the bottom medium.

We have also calculated high-order ($N=4$ iterations) scattering and emission at a higher frequency of 5 GHz. It is interesting to note that the maximum increase of the 1st order iteration can reach 50 K, and then each order iterative solutions sequentially increase as 15 K, 5 K, and 1 K. Higher iteration is not necessary.

It is also interesting to compare Fig. 8 with Fig. 6 that those locations of random cones in Fig. 8 cannot be well identified when the spatial resolution now becomes coarser e. g. $\Delta h=2.5$ m. Also, variation of brightness temperature in the whole area becomes a little smooth because coarser resolution takes the average of brightness temperature over a larger area and the whole image becomes blurred.

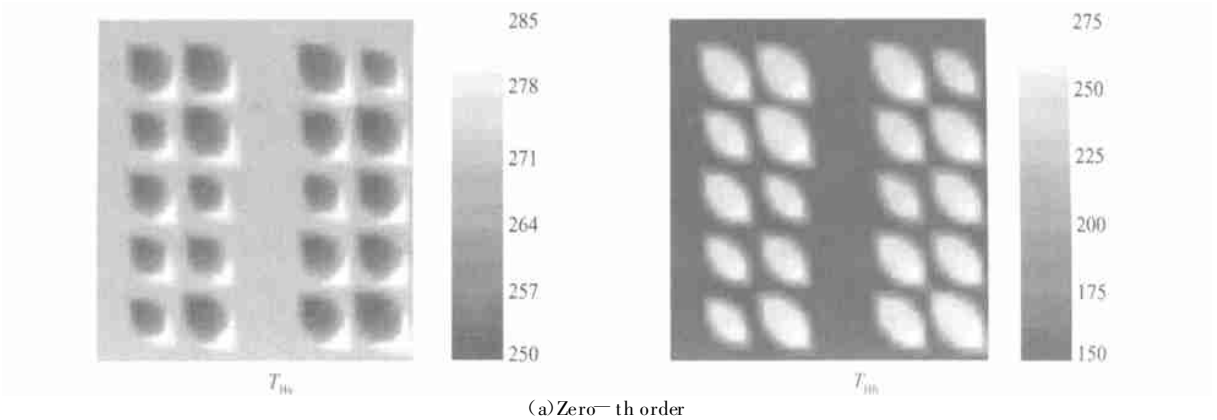

(a) Zero-th order

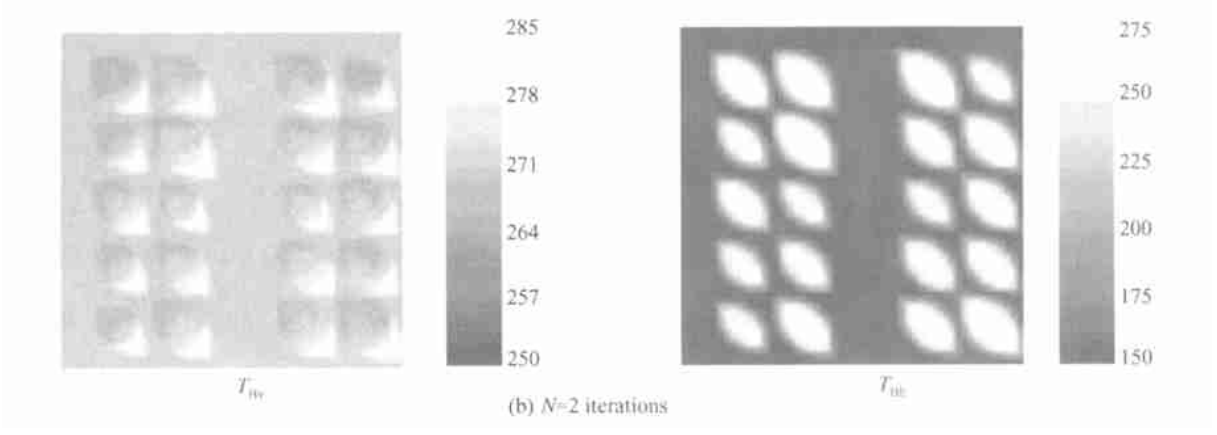

(b) N=2 iterations

Fig. 6. Brightness temperature at 3 GHz ($\theta = 58^\circ$, $\varphi = 315^\circ$).

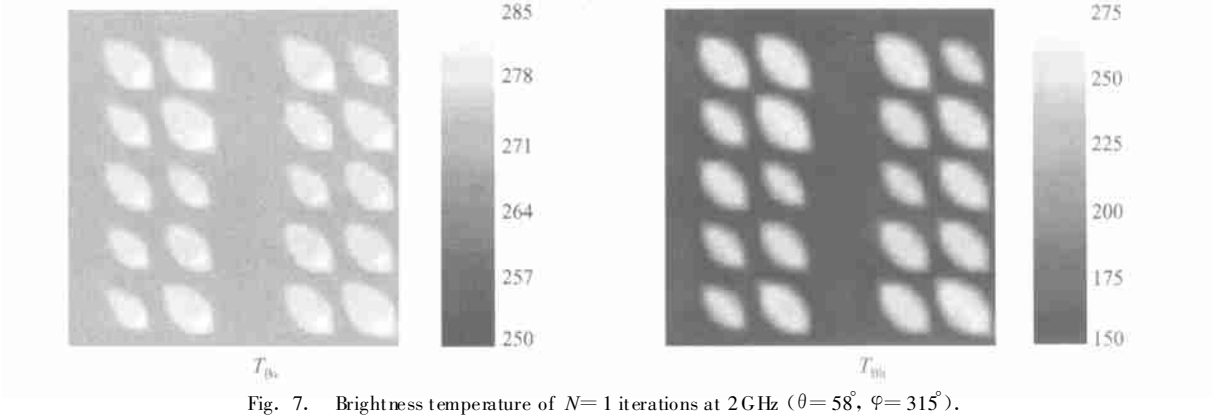

Fig. 7. Brightness temperature of N= 1 iterations at 2 GHz ($\theta = 58^\circ$, $\varphi = 315^\circ$).

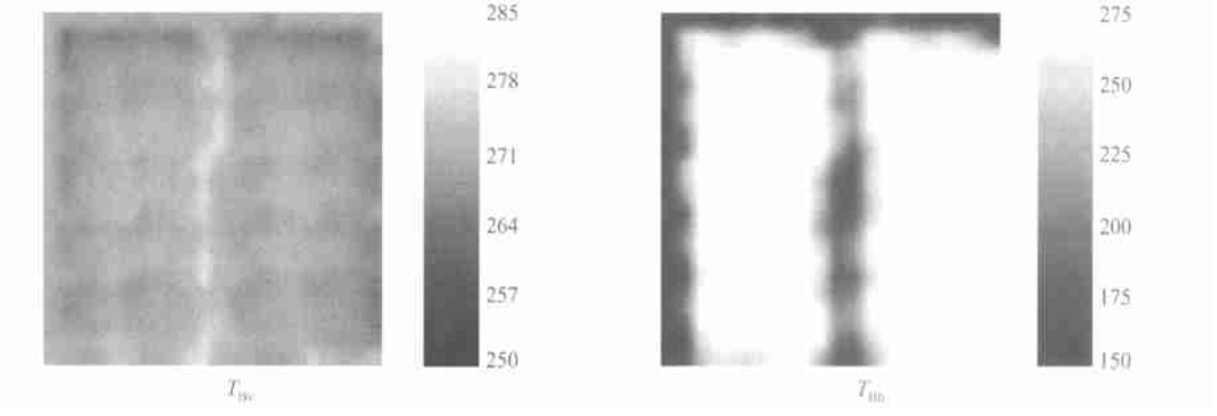

Fig. 8. Brightness temperature of N= 2 iterations for coarser resolution of 2.5 m ($\theta = 58^\circ$, $\varphi = 315^\circ$).

Our approach 3D-VRT has been validated by 1D-VRT in Fig. 5. Because the data and image for 3D case are not yet available, the validation on experimental data remains in future. However, Fig. 8 has shown how 3D-VRT can be degenerated to 1D case if the spatial resolution becomes very coarse.

4 Conclusions

An approach to solving 3-D VRT equation for spatially inhomogeneous scatter media is developed. The finite enclosure of the scatter media is divided into many thin boxes. The Mueller matrix solution of each thin box is employed for iterative algorithm of radiative transfer of the whole scatter media. Our approach of 3D-VRT is first validated by conventional 1D-VRT for the model of a homogeneous scatter medium. Numerical results of high order scattering and brightness temperature of the inhomogeneous scatter media are discussed.

According to the spatial resolution of the observation to divide the finite enclosure of scatter media, this approach presents numerical solution of high-order scattering and emission of the 3-D inhomogeneous scatter media model, e.g. for vegetation canopy, finite cloud fields etc.

References

1 Jin, Y. Q. Electromagnetic Scattering Modeling for Quantitative Remote Sensing. Singapore: World Scientific, 1994.

2 Tsang, L. et al. Polarimetric Remote Sensing. New York: Elsevier, 1990.

3 Barker, H. W. Solar radiative transfer through clouds possessing isotropic variable extinction coefficient. Q. J. Roy. Meteor. Soc., 1992, 118: 1145.

4 Evans, K. F. Two-dimensional radiative transfer in cloudy atmospheres-the soherical harmonic spatial grid method. J. Atmos. Sci., 1993, 50: 3111.

5 Dittmann, O. J. The influence of cloud geometry on continuum polarization. J. of Quantitat. Spectros. Radiat. Transfer, 1997, 57: 249.

6 Stephens, G. L. Radiative transfer in spatially heterogeneous two dimensional anisotropically scattering media. J. of Quantitat. Spectros. Radiat. Transfer, 1986, 36: 51.

7 Truelove, J. S. 3-D Radiation in absorbing-emitting-scattering media using the discrete-ordinates approximation. J. of Quantitat. Spectros. Radiat. Transfer, 1988, 39: 27.

8 Maruyama, S. et al. Improvement of computational time in radiative heat transfer of three-dimensional participating media using the radiation element method. J. of Quantitat. Spectros. Radiat. Transfer, 2002, 73: 239.

9 Sun, G. et al. A three-dimensional radar backscatter model of forest canopies. IEEE Trans. On Geosci. Rem. Sens., 1995, 33: 372.

10 Gastellu-Etchegorry, J. P. et al. Modeling radiative transfer in heterogeneous 3-D vegetation canopies. Remote Sensing of Environment, 1996, 58: 131.

11 She, Z. Three-dimensional space-borne synthetic aperture radar (SAR) imaging with multiple pass processing. Int. J. Remote Sensing, 2002, 23: 4357.

12 Chandrsekhar, S. Radiative Transfer. New York: Dover Pub., 1960.

13 Liang, Z. C. et al. Iterative approach of high-order scattering solution for vector radiative transfer of inhomogeneous random media. J. of Quantitat. Spectros. Radiat. Transfer, 2003, 77: 1.